

---

**CIplus**  
**Band 9/2016**

# **Optimization of the Cyclone Separator Geometry via Multimodel Simulation**

**Thomas Bartz-Beielstein, Horst Stenzel, Martin Zaefferer, Beate Breiderhoff, Quoc Cuong Pham, Dimitri Gusew, Aylin Mengi, Baris Kabacali, Jerome Tünste, Lukas Büscher, Sascha Wüstlich, Thomas Friesen**



## Optimization of the Cyclone Separator Geometry via Multimodel Simulation

THOMAS BARTZ-BEIELSTEIN, TH Köln  
HORST STENZEL, TH Köln  
MARTIN ZAEFFERER, TH Köln  
BEATE BREIDERHOFF, TH Köln  
QUOC CUONG PHAM, TH Köln  
DIMITRI GUSEW, TH Köln  
AYLIN MENGI, TH Köln  
BARIS KABACALI, TH Köln  
JEROME TÜNTE, TH Köln  
LUKAS BÜSCHER, TH Köln  
SASCHA WÜSTLICH, TH Köln  
THOMAS FRIESEN, TH Köln

Cyclone separators are popular devices used to filter dust from the emitted flue gases. They are applied as pre-filters in many industrial processes including energy production and grain processing facilities. Increasing computational power and the availability of 3D printers provide new tools for the combination of modeling and experimentation, which necessary for constructing efficient cyclones. Several simulation tools can be run in parallel, e.g., long running CFD simulations can be accompanied by experiments with 3D printers. Furthermore, results from analytical and data-driven models can be incorporated. There are fundamental differences between these modeling approaches: some models, e.g., analytical models, use domain knowledge, whereas data-driven models do not require any information about the underlying processes. At the same time, data-driven models require input and output data, whereas analytical models do not. Combining results from models with different input-output structure is of great interest. This combination inspired the development of a new methodology. An optimization via multimodel simulation approach, which combines results from different models, is introduced. Using cyclonic dust separators (cyclones) as a real-world simulation problem, the feasibility of this approach is demonstrated. Pros and cons of this approach are discussed and experiences from the experiments are presented. Furthermore, technical problems, which are related to 3D-printing approaches, are discussed.

CCS Concepts: • **Computing methodologies** → **Modeling methodologies**;

Additional Key Words and Phrases: Combined simulation, multimodeling, simulation-based optimization, metamodel, surrogate model, stacking, response surface methodology, 3D printing, computational fluid dynamics

### ACM Reference Format:

Thomas Bartz-Beielstein, Horst Stenzel, Martin Zaefferer, Beate Breiderhoff, Quoc Cuong Pham, Dimitri Gusew, Aylin Mengi, Baris Kabacali, Jerome Tunte, Lukas Büscher, Sascha Wüstlich, and Thomas Friesen, 2016. Optimization via Multimodel Simulation – Combining Analytical, Surrogate, CFD, and 3D-printing Modeling. *ACM V*, N, Article A (November 2016), 23 pages.  
DOI: <http://dx.doi.org/10.1145/0000000.0000000>

---

This work is supported by the *Bundesministerium für Wirtschaft und Energie* under the grants KF3145101WM3 und KF3145103WM4. This work is part of a project that has received funding from the *European Union's Horizon 2020 research and innovation program* under grant agreement No 692286.

Author's addresses: T. Bartz-Beielstein, Faculty of Computer Science and Engineering Sciences, TH Köln.

Permission to make digital or hard copies of all or part of this work for personal or classroom use is granted without fee provided that copies are not made or distributed for profit or commercial advantage and that copies bear this notice and the full citation on the first page. Copyrights for components of this work owned by others than ACM must be honored. Abstracting with credit is permitted. To copy otherwise, or republish, to post on servers or to redistribute to lists, requires prior specific permission and/or a fee. Request permissions from [permissions@acm.org](mailto:permissions@acm.org).

© 2016 ACM. 0000-0000/2016/11-ARTA \$15.00

DOI: <http://dx.doi.org/10.1145/0000000.0000000>

## 1. INTRODUCTION

Simulation is a widely used method for studying complex real-world systems, because many systems cannot be completely described by analytical (mathematical) models and experimentation with the real system is infeasible or expensive. Furthermore, simulation allows the estimation of system performance under new conditions as well as the comparison of different operating conditions and parameterizations, e.g., new geometries.

However, there are also some problems related to simulation-based approaches. Simulation models are usually more expensive than analytical models. Each simulation describes only one single setting. Several repeats with varying input data are necessary, whereas an analytical model allows the calculation of the exact characteristics of the system for several settings. An inappropriate level of model detail, failure to collect adequate system data, and using wrong performance indicators for comparisons are only three common pitfalls in simulation studies. The reader is referred to Law and Kelton [2000] for a detailed discussion of these issues.

Increasing computational power and the availability of 3D printers provide tools for new modeling approaches. Several simulations can be run in parallel, e.g., long running *computational fluid dynamics* (CFD) simulations can be accompanied by experiments with 3D printers, whereas the analytical model is evaluated as a baseline. Combinations of the following approaches are possible: (i) field experiments, (ii) lab experiments, (iii) complex simulations, (iv) model based simulations, and (v) analytical models. Two questions arise in this context:

Q-1 Are there any benefits in combining different simulation approaches?

Q-2 Can the weakness of one approach be compensated by other approaches?

To answer these questions, a methodology for combining these results is necessary. This article presents a new approach for handling several simulation models in parallel. It combines benefits from different worlds. The proposed methodology can be used as the central part of a new simulation-optimization approach [Fu 1994]. To exemplify our approach, a well established real-world simulation problem is used: cyclone dust collectors.

Cyclone dust collectors are used to filter dust from the emitted flue gases. Reverse-flow type devices with a tangential inlet (slot or wrap-around) and a cylinder-on-cone body shape will be referred to as *cyclones* in the remainder of this article. Since they are relatively simple to fabricate and maintain, cyclones are popular in many industries. Hoffmann and Stein [2007a] list the following industries, which make use of cyclones:

- oil and gas
- power generation
- incineration plants
- iron and steel industry/blast furnaces and non-ferrous industries
- ore sintering plants
- wood chip, wood mill and building material plants
- sand plants
- cement plants
- coking plants
- coal fired boilers
- lead, ferrosilicon, calcium carbide, expanded perlite, carbon black plants, etc.
- grain processing facilities such as flour mills (wheat, rice, etc.)
- ‘chemical’ plants (plastics, elastomers, polymers, etc.)
- catalyst manufacturing plants
- food industry.

The main goal of a cyclone is to filter a maximal amount of dust from the flue gas (high degree of separation), while minimizing the pressure loss. They can be applied

in extremely harsh and demanding environments, but show a relatively low separation compared to electrostatic dust collectors. If particles are larger than  $5\ \mu\text{m}$ , cyclones are efficient. Therefore, cyclones are used as pre-cleaners for other filter techniques [Swamee et al. 2009]. Many parameters determine the performance of cyclones. For practitioners, it is of importance to know which parameters are important and which are not, in any given situation. Even with today's modern tools, the complexity of cyclone behavior is such that experimental studies are necessary for a solid understanding of the phenomena governing their behavior.

Cyclones use a conical geometry to introduce a centrifugal force that separates dust from gas. The pressure drop (Euler number) and the collection efficiency are well established performance indicators for cyclones. The latter is related to the cut-off diameter (Stokes number). Both indicators are determined by several parameters, including the geometry of the cyclone. Hence, an efficient cyclone requires the optimization of the geometry parameters.

For the purpose of optimization, the performance could be estimated by full-scale, real-world experiments. Due to the extensive costs, this is not feasible. Rather, various physics-driven and data-driven models are typically used. These include (i) analytical models, (ii) CFD simulations, and (iii) metamodeling or surrogate model based approaches.

The analytical approaches developed by Barth [1956], which were further extended by Muschelknautz [1972] and co-workers, can be considered as standard in literature [Hoffmann and Stein 2007b]. This approach enables an understanding of cyclone performance as a function of its geometry, feed properties, and flow rates.

CFD simulations have proven to be useful for studying the fluid and particle flows in cyclones [Hoekstra et al. 1999; Griffiths and Boysan 1996; Gimbun et al. 2005b; Elsayed and Lacor 2010; Elsayed 2011; Gimbun et al. 2005a; Overcamp and Mantha 1998; Elsayed and Lacor 2014; Dirgo and Leith 2007; Solero and Coghe 2002; Hoffmann and Stein 2007a; Swamee et al. 2009]. They have clear advantages for understanding the details of the flow in cyclones, but also limitations in terms of modeling cyclone separation performance accurately [Hoffmann and Stein 2007a]. Numerical simulations are performed by solving the unsteady-state, three-dimensional *Reynolds averaged Navier-Stokes* (RANS) equations combined with a closure model for the turbulent stresses and the large eddy simulation approach. The physical laws governing the behavior of cyclones were established in the works of Newton and Stokes, which lay the foundations for describing the forces acting on a particle traveling in a fluid medium.

Computational fluid dynamics simulations are computationally expensive. Data-driven models of cyclone separators, which are substantially cheaper to evaluate, can be used instead. The metamodeling or surrogate-based modeling approach is well-known for accelerating optimization tasks. If a surrogate model is integrated into the optimization process, the method is referred to as *surrogate based optimization* (SBO) [Bartz-Beielstein 2016a].

As a new approach towards cyclone geometry optimization, we propose small-scale experiments, based on 3D-printed cyclones. That is, 3D-printed small-scale cyclones will be used to perform actual real-world experiments. While 3D printing reduces the cost of experiments significantly (compared to full-scale as well as complex CFD), the experiments themselves are still time-consuming and require material resources. With the cost of experiments, noise of evaluation (due to manufacturing as well as measurement inaccuracies), and the inherent complexity of the search-space due to its combinatorics, the modeling based on 3D-printed cyclones poses a major challenge. Despite of this problems, we expect combining results from the 3D-printing experiments with results from other modeling approaches might improve the overall model quality. This

improvement might (i) accelerate the optimization process and (ii) lead to new insights into the behavior of cyclones.

This article presents results from an experimental study, which combines results from various modeling approaches. The study can be regarded as a proof-of-concept for a new, integrated multimodel approach, integrating 3D-printing based modeling in the cyclone simulation and optimization loop. It combines four different modeling approaches, namely (M-A) analytical, (M-S) surrogate, (M-C) CFD, and (M-P) 3D-printing modeling.

This paper is structured as follows: Section 2 describes related work. Section 3 describes the simulation-optimization loop. Section 4 introduces cyclone design and geometry considerations. Section 5 compares results from different modeling approaches. The analytical (M-A), the surrogate modeling (M-S), the CFD modeling (M-C), and the 3D-printing (M-P) approaches are described. Experimental results are presented in Section 6. How to combine results from various models via ensemble building is shown in Section 7. Section 8 describes the metamodel-based optimization. Section 9 gives a conclusion and presents recommendations based on our experiences made in this study.

## 2. RELATED WORK

The idea of using different models with different resolution has been discussed in the literature for many years. Zeigler and Oren [1986] describe multiple levels of model aggregation (resolution, abstraction). These levels depend on the objectives, knowledge, and the available budget (resources, e.g., time). They claim that there is “an underlying unity that binds different models together—namely their common origin.” An environment “can support the integration of models so that a coherent whole emerges.” Fishwick and Zeigler [1992] present a formalism and a methodology for developing multiple, cooperative models of physical systems from qualitative physics.

Staymates et al. [2013] present the design and characterization of a streamlined, high-volume particle impactor intended for use with trace chemical analysis. Computational fluid dynamics was used as a tool to optimize the aerodynamic performance of the impactor by iteratively redesigning the geometry and curvature of the internal walls. By eliminating recirculation zones within the flowfield of the impactor and using flowfield streamlines as new walls, successive designs revealed a significant reduction in the pressure drop across the impactor. Particle trajectories were simulated in the impactor and the 50% cutpoint was determined. They fabricated a prototype impactor with a 3D rapid prototyping printer and characterized in terms of particle cut-off diameter using test aerosols generated by an Ink Jet Aerosol Generator and fluorescence intensity measurements.

Cyclone geometry and design optimization using CFD can be considered as a standard technique [Cernecky and Plandorova 2013]. The cyclone modeling, simulation, and optimization approach presented in our study is related to the work from Preen and Bull [2014], who optimized vertical-axis wind turbines using miniaturized 3D-printed wind turbines. A very general approach of integrating 3D printing into the optimization loop is presented by Eiben and Smith [2015]. These authors describe the emerging area of artificial evolution in physical systems. Chaudhuri et al. [2015] describe a flapping wing optimization task. They used multiple surrogates, multiple in-fill criteria, and multiple points for the same experimental data set to add multiple points in a cycle for optimization. In the context of real world applications, Kazemi et al. [2016] use different machine learning approaches to create simple and reliable models for predicting granule size distributions. Their models were developed based on a data set from laboratory. An iterative procedure assisted by cross validation was

implemented to find out the best model among thousands. Genetic programming and neural networks performed best.

In general, there are two options to deal with multiple models: (i) selection of the best model and (ii) combination of results from several models. Simpson et al. [2012] present a thoughtful review of several multimodel approaches. They state that “the use of multiple surrogates (i.e., a set of surrogates and possibly a weighted average surrogate) is very appealing in design optimization due to the fact that the best surrogate may not lead to the best result; and complementary because fitting many surrogates and repeating optimizations is cheap compared to cost of simulation.” Yang [2003] states that selection can be better when the errors in prediction are small and combination works better when the errors are large. Furthermore, co-kriging, which is a popular method that combines results from fine and coarse grained models, can be mentioned in this context [Forrester et al. 2007].

The approaches described so far try to select one model, whereas our approach combines results from several models using stacked regression. In addition, our approach is able to combine results from models with different run times (steady state property) [Nowostawski and Poli 1999]. The approaches mentioned above use information from surrogate models to select new design points for the manufacturing process or CFD simulation. Our study presents an integrated simulation and experimentation methodology on various scales (or layers), namely

(M-A) analytical models,

(M-S) surrogate models,

(M-C) CFD simulation, and

(M-P) 3D printing.

Simulation and optimization of cyclones were performed separately on each of these layers. To best of our knowledge, an integrated approach that combines experimentation and simulation at different levels and that uses a stacked generalization approach to generate one meta-model was not applied for this (or similar) simulation and optimization tasks. Since 3D printer become more and more affordable, evaluating the pros and cons of their integration into the simulation-optimization framework is desirable.

### 3. OPTIMIZATION VIA MULTIMODEL SIMULATION IN THE LOOP

Simulation is of great interest for practitioners planning to optimize a system, which requires the specification of a number of decision or input variables. In many situations, the input variables are also subject to constraints. Furthermore, there is an objective function to be minimized (or maximized), which is a function of one or several simulation output variables and of certain input variables. In this setting, the goal of optimization is to perform runs of the simulation model in an efficient manner and to determine those input variables, which result in an optimal (or near optimal) solution [Law and Kelton 2000; Fu 1994]. This setting is known as *optimization via simulation*. Our approach extends the standard optimization via simulation setting by integrating results from several model types. It will be referred to as *optimization via multimodel simulation* in the following.

The general concept of optimization via multimodel simulation is illustrated in Figure 1. Here, we consider the optimization of the cyclone’s geometry parameters, which should be distinguished from the process parameters. It consists of the following steps: (S-1) Select an initial design. Set  $t = 1$ , where  $t$  denotes the number of parameter sets.

The first set of parameters,  $\vec{x}_g^{(t)}$ , which describe the geometry, is generated.

(S-2) Specify the process parameters  $\vec{x}_p$ . For example, the inlet velocity and the particle size distributions have to be specified for the simulation model. The process parameters are not changed during the optimization.

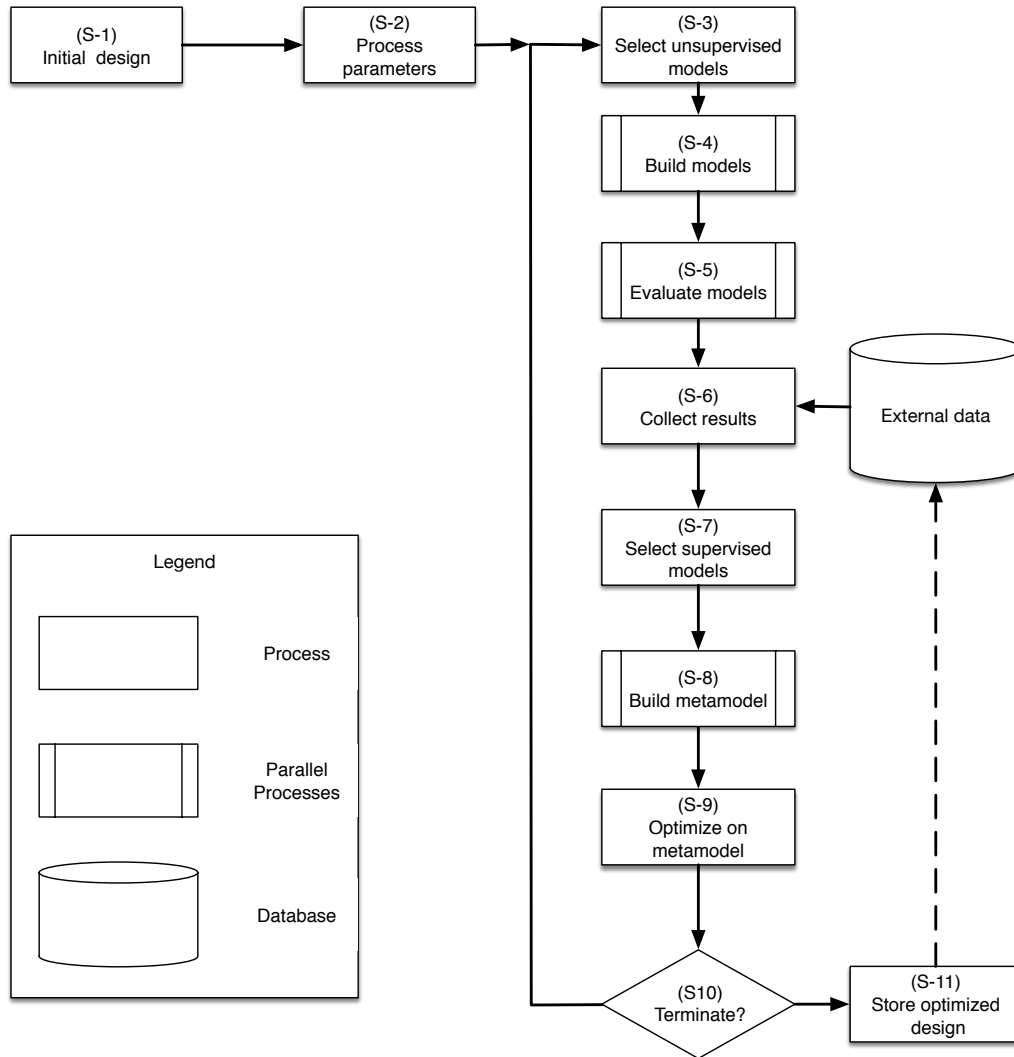


Fig. 1. Optimization via multimodel simulation in the loop. Several simulation models are used in parallel. Elements of the first set of models, i.e., during steps (S-3), (S-4), and (S-5), can be one or several CFD simulators, analytical models, or experiments based on 3D-printed objects. Results from these different models are collected and optionally combined with additional results, which were stored in a database. The second set of models is build during step (S-8). Models from the second set are classical surrogate models, e.g., neural networks, linear regression models, or Kriging models. Results from these models can be combined in several ways. We describe an approach that is based on stacked generalization [Wolpert 1992]. Optimization is performed on the stacked model (S-9).

- (S-3) Select unsupervised models (e.g., CFD, analytical). The whole parameter set,  $\vec{x}^{(t)} = (\vec{x}_g^{(t)}, \vec{x}_p)$  will be used to build the models. Note, these models are similar to unsupervised models in the machine learning community, because no information about the dependent (output) variables  $y$  is needed.
- (S-4) Build models. In this step, one or several models ( $f_1, \dots, f_p$ ) from the set of unsupervised models, which comprehends 3D-printed objects, mathematical model formulas, or CFD simulation models, are generated. The construction process results in several models, which use the same set of parameters  $\vec{x}^{(t)}$ .
- (S-5) Evaluate models. The models are evaluated, i.e., each model generates an output:  $f_j : \vec{x}^{(t)} \rightarrow y_j^{(t)}$ . Note, some models generate a deterministic output, e.g., CFD models, whereas other, e.g., 3D-printed models, generate stochastic (noisy) outputs. Therefore, repeats should be considered for the stochastic models, to improve the quality of the measured values.
- (S-6) Collect results. Besides the set of pairs  $\{(\vec{x}^{(k)}, y_j^{(k)})\}$ , for  $k = 1, \dots, t$  and  $j = 1, \dots, p$ , additional results  $\{(\vec{x}^{(m)}, y_l^{(m)})\}$ , for  $m = 1, \dots, s$  and  $l = 1, \dots, q$ , e.g., from historical data or data from the literature, can be used in the construction of the metamodels.
- (S-7) Select supervised models. The whole input parameter set,  $\vec{x}^{(t)} = (\vec{x}_g^{(t)}, \vec{x}_p)$  as well as the corresponding output values are needed for these models. In general, several design points and their corresponding output values from one or more models ( $i = 1, \dots, n$ ), i.e.,  $\{\vec{x}^{(k)}, y_i^{(k)}\}_{k=1}^s$  are mandatory for building models. For example, a simple linear regression model for seven independent variables  $\vec{x}_g = \{x_1, \dots, x_7\}$  requires eight design points ( $s = 8$ ).
- (S-8) Build metamodel. The metamodel combines information from several models, say  $F_i$ , which require the specification of independent variables,  $\vec{x}$ , and dependent variables,  $y_i$ . The metamodel will be referred to as  $F^*$ . Using methods described by Bartz-Beielstein [2016b], the models could be stacked. Instead of stacking, a weighted combination of models  $F_i$  can be used. Alternatively, co-kriging, which is also a popular method that combines results from fine and coarse grained models, can be used.
- (S-9) Optimize on the metamodel. The model  $F^*$  is used as a surrogate for performing the optimization step. The optimization results in a new set of promising geometry parameters, which will be evaluated in the following step. Therefore, the counter for the number of parameter sets  $t$  is incremented and the new design can be referred to as  $\vec{x}_g^{(t)}$ . Instead of increasing  $t$  by one, several new design points can be added to the parameter set. For a large number of experimental optimization problems, the cost of objective function evaluations plays an important role. Experiments may require time, working-hours of an operator or material resources. Hence, optimization algorithms should require as few evaluations as possible.
- (S-10) Check the termination criterion. If the budget, i.e., simulation time, is exhausted or the desired solution quality is reached, the process is stopped and the result is presented. The various models may have distinct termination criteria. For example, the availability time of a 3D printer, or the availability of material resources may be distinct from the computer simulations.
- (S-11) Store the optimized design. Optionally, it can be added to a database.

To illustrate this methodology, we will consider the cyclone optimization problem. Obviously, the optimization via simulation methodology is not restricted to the cyclone optimization problem. Results from our study can be transferred to many other applications.

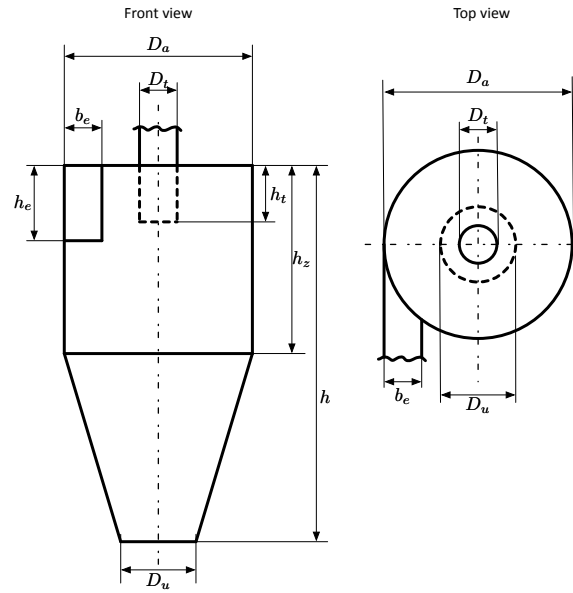


Fig. 2. Standard geometry of the cyclone considered in this study. The corresponding parameters are described in Table I.

#### 4. CYCLONE GEOMETRY AND FUNCTIONALITY

In the following, the decision variables or input parameters,  $\vec{x}_g$ , are described. The geometry of the cyclone affects the flow pattern and performance. The standard geometry of a gas cyclone is shown in Section 4. To improve reproducibility and to describe experimental setup and results as precisely as possible, important values are presented in the following tables:

- The cyclone geometry is described by the parameters shown in Table I.
- Table II shows geometries, which were found in the literature [Cortes and Gil 2007]. Values from this table were used for the analytical, surrogate, CFD modeling, and 3D-printing simulations.
- Table III presents the absolute values of the geometries, which were used in the 3D printing and CFD experiments. Each setting was repeated five times.
- Table IV shows the particle size distribution of the dust.
- Table V compares results from all modeling approaches used in this study.
- Table VI shows results from the 3D printing experiments.

We will consider cyclones with a tangential inlet, which serves to carry the dust loaded flue gas into the main separation body. Polluted air is pumped into the cyclone and two air vortices develop. Due to the tangential stimulation as well as the cylindrical / conical shape of the main body, the flue gas starts to rotate around the central axis. The outer vortex gets hold of the heavy particles. These particles sink to the bottom via gravity and fall into the receptacle. The cleansed air has to exit the cyclone because the rest of the airways are closed off. The inner vortex goes to the top and exits through the outlet pipe.

The cyclone geometry can be specified by the following parameters: inlet width  $b_e$ , body diameter  $D_a$  (alternatively: cyclone radius  $r_a$ ), diameter of the vortex finder  $D_t$

Table I. Nomenclature from [Löffler 1988]. Values (L, M, S) refers to the values of the geometry parameters  $\vec{x}_g$  for the Löffler, Muschelknautz E., and Stairmand high efficiency cyclones, respectively. The vortex finder immersion,  $h_t$ , is modified for every cyclone geometry. The type " $\vec{x}_p$ " denotes operating parameters. Parameter values, which depend on other values, are labeled as "\*" in the Type column.

Parameter	Units	Values (L, M, S)	Type	Description
$b_e$	mm	12.8; 9.92; 7.97	$\vec{x}_g$	inlet width
$D_a$	mm	80.64; 116.48; 39.97	$\vec{x}_g$	body diameter
$D_t$	mm	26.88; 29.12; 19.98	$\vec{x}_g$	diameter of the vortex finder
$D_u$	mm	26.88; 39.04; 15.04	$\vec{x}_g$	diameter of the dust exit
$h$	mm	160; 160; 160	$\vec{x}_g$	total height of the cyclone
$h_e$	mm	38.4; 29.6; 19.98	$\vec{x}_g$	inlet height
$h_t$	mm	0; 35; 44	$\vec{x}_g$	vortex finder (outlet pipe) immersion
$h_z$	mm	44.8; 29.64; 59.95	$\vec{x}_g$	cylinder height
$r_a$	mm	$D_a/2$	*	cyclone radius
$r_i$	mm	$D_t/2$	*	radius of the vortex finder
$h_i$	mm	$h - h_t$	*	height of the imaginary cylinder CS
$r_e$	mm	$r_a - b_e/2$	*	mean inlet pipe radius
$F$	-	$F_e/F_i$	*	ratio between inlet and outlet area
$F_e$	mm <sup>2</sup>	$h_e \times b_e$	*	inlet area
$F_i$	mm <sup>2</sup>	$\pi \times r_i^2$	*	outlet area
$v_e$	ms <sup>-1</sup>	20	$\vec{x}_p$	inlet velocity
$\lambda_g$	-	0.005	$\vec{x}_p$	load-free friction coefficient
$\mu$	Pa s	$1.8 \times 10^{-5}$	$\vec{x}_p$	viscosity
$\rho_f$	kg/m <sup>3</sup>	1.2000	$\vec{x}_p$	gas density
$\rho_p$	kg/m <sup>3</sup>	2700	$\vec{x}_p$	particle density
$c_{roh}$	kg/m <sup>3</sup>	0.061	$\vec{x}_p$	raw gas concentration
$B$	-	$B = c_{roh}/\rho_f$	*	mass load
$v_i$	ms <sup>-1</sup>	$\dot{V}/(\pi r_i^2)$	*	velocity vortex finder (outlet pipe)
$v_r(r_i)$	ms <sup>-1</sup>	Eq. (1)	*	radial gas velocity on the outlet pipe
$v_{\varphi i}$	ms <sup>-1</sup>	Eq. (2)	*	tangential velocity at CS
$\dot{V}$	m <sup>3</sup> /h	$F_e \times v_e$	*	volumetric flowrate through the cyclone
$\lambda$	-	$\lambda_g(1 + 2\sqrt{B})$	*	wall friction factor; friction coefficient

(alternatively: radius of the vortex finder  $r_i$ ), diameter of the dust exit  $D_u$ , total height  $h$ , inlet height  $h_e$ , vortex finder immersion  $h_t$ , and cylinder height  $h_z$ , see Table I.

Based on these input parameters, the following variables can be calculated: The inlet area  $F_e = h_e \times b_e$  and the outlet area  $F_i = \pi r_i^2$ . The ratio between inlet and outlet area is  $F = F_e/F_i$  and the ratio  $B_e = b_e/r_a$ . The mean inlet radius is  $r_e = r_a - b_e/2$ .

In addition to these geometry parameters,  $\vec{x}_g$ , the specification of the operating parameters,  $\vec{x}_p$ , is necessary. The inlet gas velocity is  $v_e = \dot{V}/F_e$ , where  $\dot{V}$  denotes the gas flow rate or the *volumetric flowrate* through the cyclone. The gas density (at 20° Celsius) is  $\rho_f$ ,  $\rho_p$  denotes the particle density, and  $\mu$  is the gas viscosity. The raw gas concentration is  $c_{roh}$ .

Last, but not least, a performance measure has to be specified. Two performance measures are widely used in low mass loading cyclones (i) the *pressure drop*, i.e., the pressure difference between the cyclone inlet and the gas exit, and (ii) the *cut-off diameter*  $x_{50}$  [Löffler 1988; Hoffmann and Stein 2007a; Elsayed 2011]. We will concentrate in this study on the collection efficiency as specified in Löffler [1988], which will be explained in Sec. 5.1.

## 5. MODELING APPROACHES

### 5.1. The Analytical Model (M-A)

A broad variety of analytical models intended to predict cyclone velocity distributions exists in the literature [Löffler 1988; Overcamp and Mantha 1998; Cortes and Gil 2007; Hoffmann and Stein 2007a]. Based on these distributions, the prediction of separation performance can be determined. For the cyclone separation models, the velocity distri-

Table II. Results from the analytical model (M-A) for cyclone geometries from Cortes and Gil [2007]. Geometries shown in the first three rows (Löffler, Muschelknautz, and Stairmand) were used for the 3D printing experiments. The height of the real cyclone,  $h_0$ , is measured in mm. All values were scaled by the height  $h_0$  of the real cyclone. Values in the last column show the efficiency. The Barth model, i.e., Eq. (5), was used to determine the collection efficiency  $E$ . It uses the process parameters from our study and the scaled geometry parameters of the original cyclones. For example, the same particle size distribution (silica sand) was used for the calculations to obtain comparable results. The last row shows the optimized geometry parameters and the estimated collection efficiency, which were obtained during the optimization on the metamodel step (S-9). This optimization is described in Section 8.

Type	$h_0$ [mm]	$h_e/h_0$	$b_e/h_0$	$D_t/h_0$	$h_t/h_0$	$h_z/h_0$	$D_a/h_0$	$D_u/h_0$	$E$
Löffler	25,000	0.2400	0.0800	0.1680	0.2600	0.2800	0.5040	0.1680	89.3334
Muschelknautz E.	934	0.1852	0.0621	0.1820	0.3330	0.1852	0.7281	0.2441	89.9122
Stairmand high eff.	1,265	0.1249	0.0498	0.1249	0.1249	0.3747	0.2498	0.0941	89.0490
Muschelknautz D.	8,630	0.2167	0.0626	0.1379	0.3685	0.3036	0.4137	0.2260	89.5968
Storch 4	16,160	0.1609	0.0235	0.0724	0.1089	0.5625	0.1609	0.0563	91.4006
Storch 3	8,210	0.2034	0.0731	0.1303	0.2436	0.5627	0.2339	0.1121	86.9871
Storch 2	10,970	0.1714	0.0483	0.0985	0.2179	0.4230	0.2051	0.0766	89.6379
Storch 1	19,430	0.0515	0.0515	0.0633	0.0726	0.2820	0.1879	0.0329	92.4774
Tengbergen C	9,300	0.1075	0.1075	0.1204	0.1559	0.2011	0.3624	0.1204	90.4930
Tengbergen B	6,040	0.2964	0.0927	0.1854	0.3709	0.5364	0.3477	0.1854	83.8606
Tengbergen A	6,470	0.2087	0.1144	0.1731	0.2427	0.2782	0.4281	0.3122	87.7651
TSN -11	9,590	0.1919	0.0563	0.1418	0.2523	0.2284	0.3629	0.1606	89.3807
TSN -15	1,1240	0.1477	0.0534	0.1406	0.3114	0.5240	0.2367	0.1059	86.6353
Stairmand high flow	7,550	0.1868	0.0940	0.1868	0.2185	0.3748	0.2517	0.0940	81.2173
Van Tongeren AC	12,310	0.1210	0.0544	0.0812	0.2640	0.3542	0.2640	0.1056	92.1290
Vibco	7,200	0.1542	0.1250	0.1542	0.1722	0.3167	0.3972	0.0917	88.6851
Lapple GP	11,310	0.1247	0.0628	0.1247	0.1565	0.5004	0.2502	0.0628	88.8657
Metamodel	160	0.1266	0.0623	0.0640	0.2929	0.1853	0.7267	0.0330	95.3494

Table III. Geometries, i.e.,  $\bar{x}_g$  values, used in the 3 D printing experiments. A total height,  $h$  of 160 mm was chosen. This table shows absolute values, which were determined using the relative values from Table II multiplied by 160. The resulting cyclones are shown in Figure 6.

Type	$b_e$	$D_a$	$D_t$	$D_u$	$h$	$h_e$	$h_t$	$h_z$
Löffler	12.8	80.64	26.88	26.88	160	38.4	0	44.8
Löffler	12.8	80.64	26.88	26.88	160	38.4	35	44.8
Löffler	12.8	80.64	26.88	26.88	160	38.4	44	44.8
Muschelknautz E.	9.92	116.48	29.12	39.04	160	29.6	0	29.64
Muschelknautz E.	9.92	116.48	29.12	39.04	160	29.6	35	29.64
Muschelknautz E.	9.92	116.48	29.12	39.04	160	29.6	44	29.64
Stairmand high eff.	7.97	39.97	19.98	15.04	160	19.98	0	59.95
Stairmand high eff.	7.97	39.97	19.98	15.04	160	19.98	35	59.95
Stairmand high eff.	7.97	39.97	19.98	15.04	160	19.98	44	59.95

bution in (i) the near-wall region, and (ii) the *control-surface* (CS), which is assumed to separate the outer region of downward flow from the inner region of upward flow, are relevant. Barth [1956] proposed a simple model to obtain the collection efficiency based on a balance of forces. The model represents a reverse flow cyclone with a tangential rectangular inlet. This is a simple and still useful model, by which friction was first introduced in cyclone modeling. It is based on the assumption that a particle carried by the vortex is influenced by two forces: a centrifugal force and a flow resistance. They are expressed at the outlet pipe radius  $r_i$  where the highest tangential velocity occurs. Some assumptions can be considered reasonable enough to obtain a good compromise between accurate prediction and simplification of the equations, e.g., the particles are spherical, the particle motion is not influenced by the presence of neighboring particles, and the radial force on the particle is given by Stokes's law.

Based on the geometry and operating parameters from Table I, the following calculations can be performed. The equilibrium-orbit model of Barth [1956], which was

extended by Muschelknautz [1972], assumes a cylindrical control surface, CS, which is constructed by extending the vortex finder wall to the bottom of the cyclone. Let  $h_i$  denote the height of CS. If  $D_u > D_t$  then  $h_i = h - h_t$ . Otherwise  $h_i < h - h_t$ . The radial velocity at  $r_i$  equals to:

$$v_r(r_i) = \frac{\dot{V}}{2\pi r_i(h - h_t)}. \quad (1)$$

For a given mass load  $B = c_{roh}/\rho_f$ , the wall friction factor or friction coefficient  $\lambda$  can be calculated as  $\lambda = \lambda_g(1 + 2\sqrt{B})$ , where  $\lambda_g = 0.005$  is the load-free friction coefficient. The correction factor  $\alpha$  for contraction, expressed as a function of the inlet geometry in case of a rectangular tangential inlet, is equal to:

$$\alpha = 1.0 - \left(0.54 - \frac{0.153}{F}\right) B_e^{\frac{1}{3}}.$$

Using the outlet pipe velocity  $v_i = \frac{\dot{V}}{\pi r_i^2}$ , Barth [1956] derived the following equation

$$\frac{v_{\varphi i}}{v_i} = U = \frac{1}{F\alpha \cdot \frac{r_i}{r_e} + \lambda \cdot \frac{h}{r_i}} = \frac{r_i r_e \pi}{\alpha F_e + h_i r_e \pi \lambda}. \quad (2)$$

These velocities are used to determine the collection efficiency. The equilibrium-orbit model is based on a force balance on a particle that is rotating at radius  $r_i$ . Small particles leave the cyclone through the vortex finder, whereas large particles are moving to the cyclone wall. The cut size,  $x_{50}$ , plays a central role in these calculations. It is analogous to the openings in a sieve. While sieving, particles larger than  $x_{50}$  will be captured, whereas smaller particles will not be captured. For cyclones, particles of size  $x_{50}$  have a 50-50 chance of being captured, smaller particles are less likely to be captured, larger particles are more likely to be captured. The forces acting on a particle rotating in CS are (i) the centrifugal force acting outward with a magnitude of  $\pi x^3 \rho_p v_{\varphi i}^2 / (6r_i)$  and (ii) the Stokesian drag acting inward  $3\pi x \mu v_r(r_i)$ . By equating these forces, Barth [1956] developed an analytical model for the cut size as follows:

$$x_{50} = \sqrt{\frac{18\mu v_r(r_i) r_i}{(\rho_p - \rho_f) v_{\varphi i}^2}}, \quad (3)$$

where  $\mu$  is the gas viscosity,  $r_i$  is the outlet pipe radius,  $\rho_p$  and  $\rho_f$  are the particle and gas densities, respectively,  $v_r(r_i)$  is the radial gas velocity on the outlet pipe as introduced in (1), and  $v_{\varphi i}$  is radial velocity of the fluid on the outlet pipe radius from (2). The reader is referred to Löffler [1988] and Hoffmann and Stein [2007a] for details of these calculations.

The fractional efficiency curve assigns an efficiency to the particle diameter as shown in Figure 3. Larger particles are collected more efficiently than smaller particles. The fractional efficiency curve is described by

$$T(x) = \left(1 + \frac{2}{\left(\frac{x}{x_{50}}\right)^{3.564}}\right)^{-1.235}, \quad (4)$$

where  $x$  is the particle size and  $x_{50}$  equals to Eq. (3). The *overall collection efficiency*  $E$  is obtained by first dividing the feed into  $N$  size fractions, each fraction comprising a known fraction of the total mass of feed solids. Next, each of these mass fractions is multiplied by the efficiency of capture for the average particle size of each fraction.

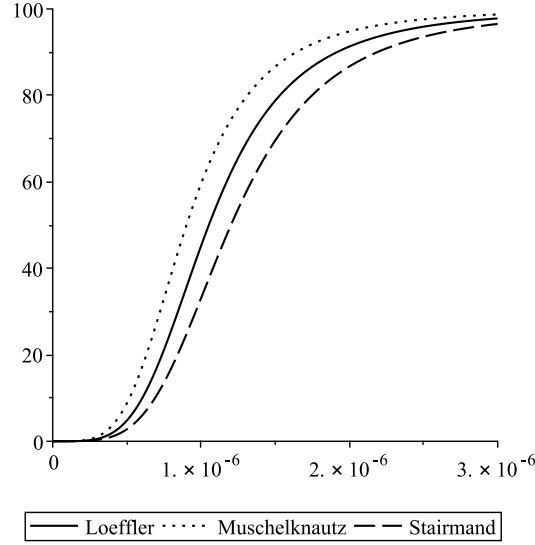


Fig. 3. Fractional efficiency,  $T(x)$ , (in %) versus particle size  $x$  in [m]. Equation (4) was used for these calculations. An immersion depth value of  $h_t = 0.044$  m was chosen. The Muschelknautz cyclone shows the best collection efficiency. This result is consistent with the results from Table V, where the Muschelknautz cyclone reaches the highest overall collection efficiency ( $E = 90.59\%$ ).

Table IV. Particle size distribution table. Values used in the 3D printing experiments

Particle Size $x$ [ $\mu\text{m}$ ]	$\Delta x$	Mean $\tilde{x}$ [ $\mu\text{m}$ ]	$\Delta Q_e(x)$	Cumulative
0-1	1	0.5	0.1	0.1
1-2.7	1.7	1.85	0.1	0.2
2.7-5.5	2.8	4.1	0.1	0.3
5.5-8.7	3.2	7.1	0.1	0.4
8.7-12.7	4	10.7	0.1	0.5
12.7-16.9	4.2	14.8	0.1	0.6
16.9-21.2	4.2	19	0.1	0.7
21.2-25.4	4.2	23.25	0.1	0.8
25.4-30.8	5.4	28.1	0.1	0.9
30.8-63	31.2	46.9	0.1	1.0

This efficiency of capture is computed with the fractional efficiency curve. The sum of all  $N$  fractions thus computed is the overall collection efficiency. The overall collection efficiency is predicted according to:

$$E = \int_{x_{\min}}^{x_{\max}} T(x)q_e(x)dx \approx \sum_{x_{\min}}^{x_{\max}} T(\tilde{x}_i)\Delta Q_e(x_i), \quad (5)$$

where  $x_{\min}$  is the lower bound of the particle size,  $x_{\max}$  is the upper bound of the particle size,  $\tilde{x}_i$  is the mean particle size in each fraction,  $\Delta Q_e(x_i) = Q_e(x_i) - Q_e(x_{i-1})$  is the change in distribution of particle sizes and  $q_e(x) = \Delta Q_e(x_i)/\Delta x_i$ . The particle size distribution table, which was used in our studies, is shown in Table IV.

Results from the calculations of the overall collection efficiency, which were based on the analytical model, are shown in column (M-A) in Table V.

### 5.2. Surrogate Modeling (M-S)

A well-known approach to handle costly objective functions is to employ surrogate models [Jin 2003]. That is, data-driven surrogate models may be constructed based on experimental results. Then, an optimization algorithm may work on the surrogate model instead of the actual objective function.

Data from Table II can be used to fit a surrogate model, which is able to predict the collection efficiency. For example, if a standard linear regression with variable selection is performed, the following model is obtained:

$$E = 95.54 + 26.10h_e - 27.77b_e - 596.19D_t - 24.40h_t + 110.80D_a. \quad (6)$$

The diameter of the vortex finder and the cyclone body diameter have the greatest effect on the collection efficiency. Although this model already shows good accuracy, e.g., adjusted  $R$ -squared 0.93, more sophisticated linear models or Kriging models can be fitted [Turner et al. 2013], [Kleijnen 2014]. Optimization can be performed on this model, e.g., to improve the collection efficiency for a given pressure drop. Even multi-objective optimization techniques can be applied [Elsayed and Lacor 2012; Zaefferer et al. 2014].

### 5.3. CFD Simulations (M-C)

The CFD simulations were carried out with the open source software OpenFOAM, which has been developed for solving numerical problems [Konan and Huckaby 2015]. The mesh for these CFD simulations consists of approximately 30,000 to 50,000 hexahedral cells. The transient MPPICFoam solver was chosen to calculate the two-phase flow (Euler-Lagrange). The OpenFOAM cyclone tutorial [OpenFOAM Foundation 2016] was used as a basis. The settings for fvSchemes, fvSolution, transportProperties, and turbulenceProperties were adapted to obtain the same setup as for the 3D printing experiments. The settings in the kinematicCloudProperties file were adjusted to the characteristics of the used particles. The density of the particles was changed to 2,700 kg/m<sup>3</sup> (as in Table I above).

Using the generalDistribution model, the particle distribution (described in Table IV) can be precisely mapped. In the simulations 20,000 parcels represent the entirety of the particles, where each parcel has the same mass. The amount of 20,000 parcels was chosen to minimize the represented mass per parcel and not to blow up the calculation time for each timestep. The minimization causes a lower error when a parcel escapes at an outlet. There is a total of 0.6 g particles, which are uniformly distributed over the inlet area.

The heatTransfer, surfaceFilm, damping, stochasticCollision, and radiation sub-models were left unchanged at the “off” state. In the experiments, a total of 6 g was spread over 10 thrusts and the waiting time between each thrust was approximately 3 seconds. The simulation takes only one thrust of 0.6 g instead of performing the 10 repetitions. The purpose of this was to avoid an extrem long simulation time. The particle velocity in the simulation was set to the same value as the determined velocity of the air at the inlet.

Using the setting “duration”, the amount of injected parcels per iteration was indirectly adjusted to ensure that only one parcel per iteration was injected.

Overall, a time frame of 3 seconds is simulated. For this, a total calculation time of approximately 96 hours using 16 processor cores is required. The simulation was controlled by the time step and relaxation factors and behaved relatively stable. The evaluation of the simulation results is shown in column (M-C) in Table V.

Table V. Summary of the results from different modeling approaches. Overall collection efficiency  $E$  (in %) as defined in Eq. 5 for three different cyclone types, three different outlet pipe immersions ( $h_t$ ), and four different modeling approaches (M-A), (M-C), (M-P), and (M-S). 3D-print column (M-P) shows mean (and standard deviation) from five repeats. The column (M-P\*) contains the same values as (M-P), where three obvious outliers were removed. Values in column (M-S) are based on Eq. (6).

Type	$h_t$	(M-A)	(M-C)	(M-P)	(M-P*)	(M-S)
Löffler	0	90.19	97.98	86.8( $\pm 4.39$ )	86.8( $\pm 4.39$ )	89.80
Löffler	35	89.49	97.89	94.5( $\pm 6.92$ )	92.13( $\pm 5.12$ )	88.95
Löffler	44	89.27	98.03	90.83( $\pm 3.84$ )	90.83( $\pm 3.84$ )	88.73
Muschelknautz	0	91.14	97.37	72.53( $\pm 17.79$ )	78.92( $\pm 12.27$ )	92.13
Muschelknautz	35	90.37	97.92	86.83( $\pm 9.55$ )	86.83( $\pm 9.55$ )	91.28
Muschelknautz	44	90.15	98.15	92.87( $\pm 2.94$ )	92.87( $\pm 2.94$ )	91.06
Stairmand	0	89.33	96.17	90.53( $\pm 5.68$ )	90.53( $\pm 5.68$ )	88.79
Stairmand	35	88.70	97.8	95.43( $\pm 2.81$ )	94.29( $\pm 1.34$ )	87.93
Stairmand	44	88.45	97.8	95.5( $\pm 2.5$ )	95.5( $\pm 2.5$ )	87.71

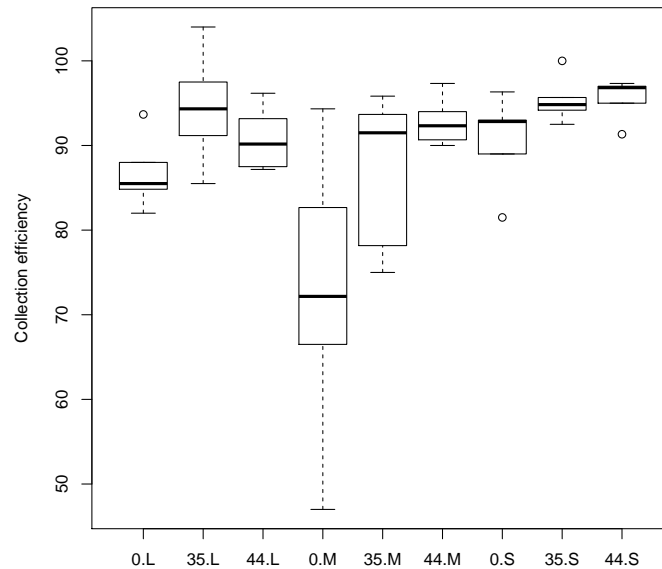


Fig. 4. Box plots of the 3D-print data. The data are grouped according to  $h_t \in \{0, 33, 45\}$  and cyclone type (L = Löffler, M= Muschelknautz, S= Stairmand). The y-axis shows efficiency (%).

#### 5.4. 3D-printing Model (M-P)

Experiments used standard laboratory equipment: Erlenmeyer flask, stand, pressure gauge, precision scale, and a vacuum cleaner. The experimental setup is illustrated in Figure 5.

The init step (S-1) comprehends the selection of an initial design,  $\vec{x}_g$ . This design is also used for other model types, e.g., (M-C) and (M-A). If no experimental data is available, standard geometries from the literature as shown in Table II can be used as starting points. Design of experiment methodology can be used if planned experiments are possible. Table III shows the parameters of the printed cyclones. Process parameters,  $\vec{x}_p$ , as described in Table I are used in addition.

The model building step (S-3) consists of the (i) 3D computer model generation and the (ii) printing step. The 3D models, described in the *STereoLithography, Standard*

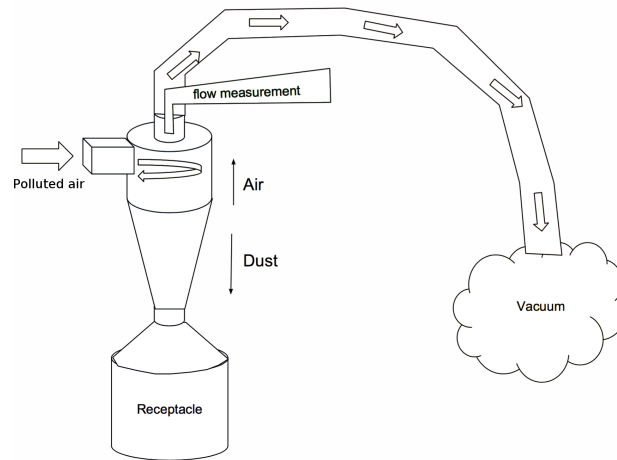


Fig. 5. Experiments using the 3D-printing model as described in Section 5.4. Schematic illustration of the experimental setup.

*Tessellation Language* (STL) are created using a Python script.<sup>1</sup> The Python script uses the FreeCad Python library.<sup>2</sup> The script creates a cyclone based on the geometry parameters. Construction of composite objects is straightforward. For example, first a function to generate a solid body with a given height, diameter, and position is used. To generate a hollow object, a second slightly bigger cylinder is created and the difference of both is computed. The resulting object is a hollow pipe with the specified wall thickness and height. The cylinder has to be fused to all other parts, so the model is one printable object and not a collection of separate parts. Finally, the model is exported to an .STL file. The .STL format is a 3D model which can be printed on a broad number of 3D printers. The three derived cyclone models are shown in Figure 6.

Today, a broad variety of 3D printers as well as different materials are available to print the cyclone. The printing technique as well as the material have to meet certain requirements. The cyclone has to be robust, because it is fixed into position for the experiments and it has to withstand the flow of air and dust. Due to the hollow shape of the cyclone a ProJet CJP 660pro printer was chosen, which uses gypsum powder (Visijet PXL) as printing substrate. This way the entire cyclone can be printed in one step, no support structures have to be removed, and it is not necessary to assemble the printer from parts which would leave seams that could hinder the air flow. The gypsum powder has to be hardened after surplus gypsum powder has been removed from the interior. A problem that could arise is buildup of static charge in the cyclone. If the material is statically charged and the dust adheres to it, the results are unusable, because it leads to fluctuations and reduced efficiency. That is why we used cyan acrylate (“ColorBon”), which yielded a sufficiently smooth, though still somewhat rough surface, at the same time giving the cyclone sufficient stability. While many real-world cyclones have to deal with hot flue gases, the experiments were performed at room temperature. Significantly higher temperatures may require a different choice of material.

<sup>1</sup><https://www.python.org/>

<sup>2</sup><http://www.freecadweb.org>

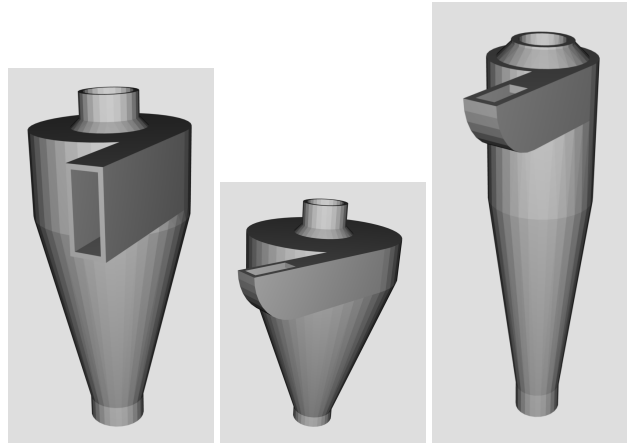


Fig. 6. From *left to right*: Löffler, Muschelknautz, Stairmand cyclones. The corresponding geometries,  $\vec{x}_g$ , are specified in Table III.

Printing a single cyclone model this way takes about three hours for the printing process, one hour for refinishing, dust removal and infiltration, and another hour for curing.

Besides the selection of a printer and material, the characteristics of the dust have to be selected. The distribution of particle sizes should not vary to prevent fluctuations in the results. If the particles are too large, they may be too easy to separate from the gas. If there are too many, they may even block the flow inside the cyclone. If the particles are too small, the task of separation may become near to impossible. The chosen dust is silica sand with a maximal particle size of  $63\mu\text{m}$ . Its particle size distribution is shown in Table IV.

Furthermore, the measurements have to be clearly specified. The same amount of dust, here: 6 g, has to be used in every experiment. The amount of dust filtered out of the air determines the efficiency of a cyclone. It can either be measured by the amount in the air after it passes through or by the amount in the receptacle. It is easier to measure the second option. The air pressure has to be the same in each test. Otherwise the results are not comparable. It can be measured in front or behind the cyclone.

To measure the efficiency of different cyclones, the cyclones have to be interchangeable. The depth of the outlet pipe can be variable. The dust receptacle has to be removable to measure its contents after a test. The rest of the setup is fixed to minimize fluctuations.

The experiments were performed following a standardized five-step procedure, which can be summarized as follows:

- (1) The cyclone is put into position at the desired outlet pipe depth.
- (2) The weight of the receptacle is measured and used as a starting point for the following tests. The receptacle is then put into position and sealed. Meanwhile 6g of dust, with a tolerance of 0.05g, are prepared.
- (3) The vacuum cleaner is started. The pressure gauge takes some time to measure. If the pressure is off, the sealing between the connection is checked. The setup is then adjusted until the pressure reaches an acceptable level.
- (4) A constant rate of the dust is then put into the cyclone through the inlet pipe. After all dust is inserted, the cyclone takes a few seconds to process the air. The vacuum cleaner is then turned of.

Table VI. Results from the 3 D printing experiments (M-P). Determination of the collection efficiency of the Löffler cyclone with  $\bar{x}_g$  taken from Table III. Similar results were obtained for the Muschelknautz and the Stairmand cyclones.

Receptacle before (g)	Receptacle after (g)	Difference (g)	Depth outlet pipe (mm)	Efficiency (%)	Average (%)
415.35	420.44	5.09	0	84.83	
420.44	425.36	4.92	0	82	
425.36	430.64	5.28	0	88	
430.64	436.26	5.62	0	93.67	
436.26	441.38	5.13	0	85.5	86.8(±4.39)
387	392.13	5.13	35	85.5	
392.13	397.6	5.57	35	91.17	
397.6	403.45	5.85	35	97.5	
403.45	409.69	6.24	35	104	
409.69	415.35	5.66	35	94.33	94.5(±6.92)
359.66	364.89	5.23	44	87.17	
364.89	370.23	5.25	44	87.5	
370.23	375.64	5.41	44	90.17	
375.64	381.23	5.59	44	93.17	
381.23	387	5.77	44	96.17	90.83(±3.84)
All					90.71

(5) The receptacle is removed and weighed again. The difference between the starting weight and the second weight is calculated. The result shows how efficient the cyclone worked. The second weight is used as the base weight for the next test. Results from the 3D-printing experiments are shown in column (M-P) in Table V. Box-plots, which visualize these results are shown in Figure 4.

## 6. EXPERIMENTAL RESULTS

We discuss results from the 3D printing (M-P) experiments first. As can be seen in Table VI, the efficiency of the Löffler cyclone is approximately 90%. Two measurements with high efficiency values (104% and 97.5%) are listed in this table. This can be a results of insufficient cleaning of the cyclone between tests. The pressure might also lead to slightly higher or lower efficiency, because it has to be modified during experimentation. The highest average efficiency (94.5%) was reached with a depth of 35mm. Zero immersion depth lead to the lowest result (86,8%).

Summarized results from the experiments with the Muschelknautz cyclone are shown in Table V. The efficiency of the Muschelknautz cyclone is around 84%. Extreme outliers can be found at a depth of 0mm. The results at 35mm depth fluctuate heavily as well. The best average efficiency is reached with a depth of 44 mm. The efficiency lowers relative to the depth, as can be seen in Figure 4.

According to the (M-P) column in Table V, the Stairmand cyclone has the highest average efficiency. The efficiency at every depth is higher than the previous two cyclones with the same depth. There are fewer fluctuations in the results. The only outliers can be found at the beginning of every series of tests. These outliers may be caused by dust particles from previous experiments. The cyclone has no large difference between a depth of 35 and 44 mm, as can be seen in Figure 4.

After removing obvious outliers, e.g., efficiencies larger than 100%, the values from column (M-P\*) were obtained. Results from the 3-D printing experiments (M-P) can be summarized as follows: (i) there are high variances in the measured values, and (ii) the experimental results indicate that the collection efficiency,  $E$ , increases with increasing vortex finder immersion ( $h_t$ ) values.

In addition to the discussion of the results from the 3D printing experiments, we consider results from the CFD simulations and from the analytical model. Efficiency

values, which are based on the CFD simulations are generally higher than values from other simulations. Again, there are high variances in the measured values, and the experimental results indicate that the collection efficiency increases with increasing vortex finder immersion values. Interestingly, data from the analytical model (M-A) show a negative effect of the immersion length,  $h_t$ , on the efficiency: smaller  $h_t$  values result in an increased collection efficiency  $E$ .

Overall, there are several inconsistencies in the data that have to be clarified. The required steps to fix these problems are obvious: the variance in the (M-P) model can be reduced by improving the experimental procedure, e.g., by keeping the operating parameters constant during experimentation. Additional recommendations will be presented in Section 9. However, even if the data itself do not enable to draw reliable conclusions for designing an optimal cyclone geometry, they are suitable for demonstrating the optimization via multimodel simulation approach.

## 7. ENSEMBLE BUILDING

Step (S-8) of the proposed methodology uses an *ensemble engine* to combine results from several models. It uses the collected results from step (S-6). In contrast to the model types used in steps (S-3) to (S-5), the models in step (S-8) require data with input and output values. This corresponds to supervised learning in machine learning. It can be briefly outlined as follows: The rich variety of surrogate models includes approaches such as regression trees and random forest, *least angle regression* (LARS), and Kriging. The ensemble engine uses cross validation to select an improved model from the portfolio of candidate models [van der Laan and Dudoit 2003]. It implements methods for creating a weighted combination of several surrogate models to build the improved model and methods, which use stacked generalization to combine several level-0 models of different types with one level-1 model into an ensemble [Wolpert 1992]. The level-1 training algorithm is typically a relatively simple linear model. The stacked generalization approach is detailed in Bartz-Beielstein [2016b]. As level-0 models, a simple regression model (lm), a regression tree (tr), a random forest (rf), and a Kriging (kr) model were used in this study. The level-1 model, which combines results from the level-0 models, uses the following coefficients:

$$\text{Ensemble (level-1)} : -213.41 + 0.31 \text{ lm} + 0.77 \text{ rf} - 1.95 \text{ tr} - 0.45 \text{ kr}$$

i.e., the stacked model uses mainly the information from the regression tree (tr) surrogate (level-0) model, but includes information from the other surrogate models as well.

## 8. METAMODEL-BASED OPTIMIZATION

The metamodel  $F^*$  from Section 7 can be used for optimizing the geometry parameters  $\vec{x}_g$ . This is step (S-9) in the optimization via multimodel simulation approach. To illustrate the optimization step, the R package SPOT2 can be used. The package SPOT2 is the most recent version of the *sequential parameter optimization* (SPO), which implements several tools for the analysis and optimization of complex problems. It combines methods from *design of experiments*, *response surface methodology*, *design and analysis of computer experiments*, and regression trees for the analysis of algorithms [Bartz-Beielstein et al. 2005]. The R script `bart16eOptimizationViaMultimodelSimulation.R`, which explains the optimization step can be downloaded from the author's webpage. On the same page, the SPOT2 package can be found.

After collecting results (step S-6) from the different models, e.g., (M-P), (M-C), or (M-A), the results are collected and can be loaded as an R data.frame. A set of surrogate models have to be chosen (step S-7). To exemplify this step, a linear regression model, a random forest, a regression tree and a Kriging model, were chosen. The SPO2 function

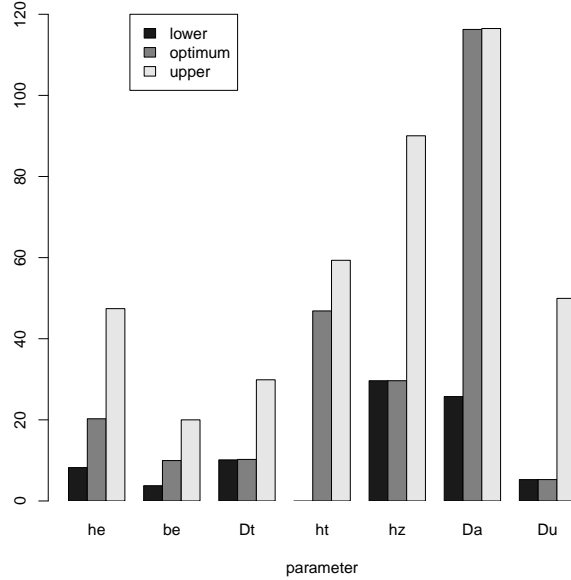


Fig. 7. Optimization on the metamodel (S-9). Barplot of the optimized geometry parameters. Comparing lower and upper bound of decision space with optimum.

`buildEnsembleStack` implements the metamodel building step (S-8). After generating an objective function from the fit, an optimizer can be applied. In our example, differential evolution was used, but any other optimizer is fine.

Results from the optimization are as follows:  $h_e = 0.13$ ,  $b_e = 0.06$ ,  $D_t = 0.06$ ,  $h_t = 0.29$ ,  $h_z = 0.19$ ,  $D_a = 0.73$ ,  $D_u = 0.03$ . All values are relative to the cyclone height  $h_0 = 160\text{mm}$ . This geometry results in an estimated efficiency of 95.35%. The values are also shown in the last row of Table II. Results from this optimization are shown in Figure 7. This figure illustrates the recommendations from the optimization on the metamodel. For example, the immersion length,  $h_t$ , should be increased, whereas the diameter of the vortex finder,  $D_t$  should be decreased.

If the termination criteria are not fulfilled, these recommendations can be used to print a new cyclone (M-P) or to perform a CFD simulation and start the next iteration of the optimization via multimodel simulation loop as introduced in Figure 1.

## 9. CONCLUSIONS

This article explores a new approach for combining different simulation approaches. Based on a stacking, a flexible methodology for combining results from different models is presented. It is demonstrated, how results from two different modeling approaches, namely,

- (1) models that require only input values, i.e. (M-A), (M-P), and (M-C), and
- (2) models, that require input and output values, i.e., (M-S),

can be combined. If data is scarce and simulation is expensive, the proposed *optimization via multimodel simulation* is a promising way. However, research question (Q-1) “Are there any benefits in combining different simulation approaches?” cannot be con-

clusively answered. The experimenters, who carried out the 3D printing experiments, faced unpredictable technical difficulties. Experience from practice plays a crucial role for these experiments. First results indicate that the weakness of one approach can be compensated by other approaches, but needs further investigations. This question was formulated as research question (Q-2) in the introduction.

This remainder of this article summarizes important experiences from our study. First, we discuss problems related to the 3D-printing approach. Then, we will discuss the optimization via multimodel simulation approach.

### 9.1. Technical Recommendations (3D-printing)

One important goal of this study was the exploration of difficulties integrating a 3D-printing approach into the optimization loop, using utilities from a standard laboratory.

- (1) It was possible to 3D print working cyclones with varying parameters. Once the procedure is clarified, it is easy (but time consuming) to create new cyclones.
- (2) One possible problem is the used material in the 3D-printing process. The chosen material has a rather rough texture, which collects dust and produces fluctuating results. A better alternative would be a smoother surface. This can be achieved through a different material, sealing the rough surface or modifying the printing process.
- (3) There were high fluctuations in the results because the cyclones were not cleansed of dust after each tests. Doing so would have resulted in a high workload and spreading the dust in the lab.
- (4) Guaranteeing a constant air pressure was a difficult task. Fluctuations in the pressure caused high variance in the experimental results. The used pressure might be too low for usable results. A higher pressure would require a pressure gauge that can measure in a higher range to ensure that the pressure stays constant.
- (5) The chosen dust has a specific size distribution. Other material, e.g., sawdust, might need higher pressure to flow through the cyclone. This is because different dust particles can have varying size, shape, or density.
- (6) The sealing could be improved and the suction power should be kept constant.
- (7) While testing the first cyclone (Löffler), it was hard to insert the dust into the cyclone. To simplify the infill procedure new cyclones were printed with rounded opening that points to the top. This design was chosen, because it does not affect the flow inside and makes it easier to insert dust. The different cyclones were then measured for their efficiency in a series of tests. It would also be beneficial to find an automated, more uniform dust insertion procedure.
- (8) The cyclones that were printed are of small size. Larger cyclones ( $h > 200$  mm) might result in a robust behavior of the cyclone.

Besides these technical difficulties from the 3D-printing approach, there are additional problems, which refer to the other models as well. Recommendations based on our experiences can be listed as follows.

### 9.2. Statistical Recommendations

- (1) Collection efficiency values, which are based on the analytical model (M-A) and the 3D-printing models are in the same range (approximately 90%). Surprisingly, values from the CFD-based models (M-C) are significantly higher. These results indicate, that a model validation is necessary. Validation analyzes the authenticity of the model, i.e., how closely the model represents a real system. Model assumptions are reviewed by experts, various data settings are tested, and independent test data are used for comparison [Law and Kelton 2000].

- (2) Experiments should be repeated if unusual values occur. Or, these data should not be considered if a plausible explanation for this behavior can be given. Only a very moderate data preprocessing was performed in this study. For example, experimental results which are very implausible were removed. This results in the values reported in column (M-P\*) in Table V. Each experiment was repeated five times. As a rule of thumb, we recommend that each experiment should be repeated at least ten times.
- (3) It was not possible to determine a rule of thumb for an efficient cyclone. The results show that there was no perfect cyclone, but some cyclones were better at different outlet pipe depths. Based on columns (M-C) and (M-P) from Table V, the Stairmand cyclone with 35 and 44 mm immersion depth has a higher efficiency than the other cyclones. A depth of 0 mm usually produces higher fluctuations than a depth of 35 or 44 mm. Although results are approximately in a similar range (90-95%), no valid conclusions could be drawn based on these data.

The results of the proof of concept show the validity of the optimization via multimodel simulation approach. Due to insufficient experience with the experimental setup, the results in this area are not yet conclusive, but they demonstrate how to collect data and how to combine results from different modeling approaches.

This study was considered as a proof-of-concept for the optimization via multimodel simulation approach. All steps of the simulation-optimization framework were tested and evaluated. As a consequence of the positive evaluation of this framework, future work should deal with an extensive optimization via multimodel simulation study, which focuses on the improved cyclone geometries.

## APPENDIX

In this appendix, we describe the supplementary R source files and the set of experimental data, which was used in our study.

- (1) `Bart16eAllData.csv`: This CSV file contains all data used in this study.
- (2) `SPOT2.0.1.tar.gz`: R software package required for running the analysis. To install the package from source, you can either use the R-command-line call:  

```
install.packages(pkgs="SPOT2.0.1.tar.gz", repos=NULL, type="source")
```

Or you can use the RStudio IDE to install via "Tools - Install Packages ...". Note, that you may require RTools if you install source packages under Windows: <https://cran.r-project.org/bin/windows/Rtools/>.
- (3) `bart16eEda.R`: This R script was used to generate the boxplots and to calculate means and standard deviations of the 3D-printing data, i.e., columns (M-P) and (M-P\*), in Table V.
- (4) `bart16eOptimizationViaMultimodelSimulation.R`: This R script was used to build the metamodel and to run the optimization step (S-9) on the metamodel  $F^*$ . The R functions, which are necessary for building the metamodel, are implemented in the R package SPOT2.

The source files and the open source R software package SPOT2 can be downloaded from the author's webpage: <http://www.gm.fh-koeln.de/~bartz/Bart16e.d>. The software package SPOT2 will also be made available on CRAN (<https://www.r-project.cran.org>).

## REFERENCES

- Walter Barth. 1956. Berechnung und Auslegung von Zyklonabscheidern aufgrund neuerer Untersuchungen. *Brennstoff-Wärme-Kraft* 8, 1 (1956), 1–9.
- Thomas Bartz-Beielstein. 2016a. A Survey of Model-Based Methods for Global Optimization. In *Bioinspired Optimization Methods and their Applications*, Gregor Papa and Marjan Mernik (Eds.). 1–18.

- Thomas Bartz-Beielstein. 2016b. *Stacked Generalization of Surrogate Models - A Practical Approach*. Technical Report 5/2016. TH Köln, Köln.
- Thomas Bartz-Beielstein, Christian Lasarczyk, and Mike Preuss. 2005. Sequential Parameter Optimization. In *Proceedings 2005 Congress on Evolutionary Computation (CEC'05), Edinburgh, Scotland*, B McKay et al. (Eds.). IEEE Press, Piscataway NJ, 773–780.
- Josef Cernecky and Katarina Plandorova. 2013. The effect of the introduction of an exit tube on the separation efficiency in a cyclone. *Brazilian Journal of Chemical Engineering* 30, 3 (2013), 627–641.
- Anirban Chaudhuri, Raphael T. Haftka, Peter Ifju, Kelvin Chang, Christopher Tyler, and Tony Schmitz. 2015. Experimental flapping wing optimization and uncertainty quantification using limited samples. *Structural and Multidisciplinary Optimization* 51, 4 (2015), 957–970.
- Cristobal Cortes and Antonia Gil. 2007. Modeling the gas and particle flow inside cyclone separators. *Progress in Energy and Combustion Science* 33, 5 (Oct. 2007), 409–452.
- John Dirgo and David Leith. 2007. Cyclone Collection Efficiency: Comparison of Experimental Results with Theoretical Predictions. *Aerosol Science and ...* 4, 4 (June 2007), 401–415.
- Agoston E Eiben and Jim Smith. 2015. From evolutionary computation to the evolution of things. *Nature* 521, 7553 (May 2015), 476–482.
- Khairy Elsayed. 2011. *Analysis and Optimization of Cyclone Separators Geometry Using RANS and LES Methodologies*. Ph.D. Dissertation.
- Khairy Elsayed and Chris Lacor. 2010. Optimization of the cyclone separator geometry for minimum pressure drop using mathematical models and CFD simulations. *Chemical Engineering ...* 65, 22 (Nov. 2010), 6048–6058.
- Khairy Elsayed and Chris Lacor. 2012. CFD modeling and multi-objective optimization of cyclone geometry using desirability function, artificial neural networks and genetic algorithms. *Applied Mathematical Modelling* 37, 8 (2012), 5680–5704.
- Khairy Elsayed and Chris Lacor. 2014. Analysis and Optimisation of Cyclone Separators Geometry Using RANS and LES Methodologies. In *Turbulence and Interactions*. Springer Berlin Heidelberg, Berlin, Heidelberg, 65–74.
- Paul A Fishwick and Bernard P Zeigler. 1992. A multimodel methodology for qualitative model engineering. *ACM Transactions on Modeling and Computer Simulation* 2, 1 (Jan. 1992), 52–81.
- Alexander Forrester, András Sóbester, and Andy Keane. 2007. Multi-fidelity optimization via surrogate modelling. *Proceedings of the Royal Society A: Mathematical, Physical and Engineering Science* 463, 2088 (2007), 3251–3269.
- Michael C Fu. 1994. Optimization via simulation: A review. *Annals of Operations Research* 53, 1 (Dec. 1994), 199–247.
- Jolius Gimbut, T G Chuah, Thomas S Y Choong, and A Fakhru'l-Razi. 2005a. A CFD Study on the Prediction of Cyclone Collection Efficiency. *International Journal ...* 6, 3 (July 2005), 161–168.
- Jolius Gimbut, T G Chuah, A Fakhru'l-Razi, and Thomas S Y Choong. 2005b. The influence of temperature and inlet velocity on cyclone pressure drop: a CFD study. *Chemical Engineering and Processing: Process Intensification* 44, 1 (Jan. 2005), 7–12.
- W D Griffiths and F Boysan. 1996. Computational fluid dynamics (CFD) and empirical modelling of the performance of a number of cyclone samplers. *Journal of Aerosol Science* 27, 2 (March 1996), 281–304.
- A J Hoekstra, J J Derksen, and H E A Van Den Akker. 1999. An experimental and numerical study of turbulent swirling flow in gas cyclones. *Chemical Engineering ...* 54, 13-14 (July 1999), 2055–2065.
- Alex C Hoffmann and Louis E Stein. 2007a. *Gas Cyclones and Swirl Tubes*. Springer Berlin Heidelberg, Berlin, Heidelberg.
- Alex C Hoffmann and Louis E Stein. 2007b. The Muschelknautz Method of Modeling. In *Gas Cyclones and Swirl Tubes*, Alex C Hoffmann and Louis E Stein (Eds.). Springer Berlin Heidelberg, Berlin, Heidelberg, 111–137.
- Y Jin. 2003. A comprehensive survey of fitness approximation in evolutionary computation. *Soft Computing* 9, 1 (Oct. 2003), 3–12.
- Pezhman Kazemi, Mohammad Hassan Khalid, Jakub Szlek, Andreja Mirtič, Gavin K Reynolds, Renata Jachowicz, and Aleksander Mendyk. 2016. Computational intelligence modeling of granule size distribution for oscillating milling. *Powder Technology* (July 2016).
- Jack P C Kleijnen. 2014. Simulation-optimization via Kriging and bootstrapping: a survey. *Journal of Simulation* 8, 4 (May 2014), 241–250.
- A Konan and D Huckaby. 2015. Modeling and simulation of a gas-solid cyclone during an upset event (Presentation). OpenFOAM Workshop 2015. (June 2015).
- A M Law and W D Kelton. 2000. *Simulation Modeling and Analysis* (3rd ed.). McGraw-Hill, New York NY.

- Friedrich Löffler. 1988. *Staubabscheiden*. Thieme, Stuttgart.
- Edgar Muschelknautz. 1972. Die Berechnung von Zyklonabscheidern für Gase. *Chemie Ingenieur Technik* 44, 1-2 (Jan. 1972), 63–71.
- Mariusz Nowostawski and Riccardo Poli. 1999. Parallel Genetic Algorithm Taxonomy. In *Knowledge-Based Intelligent Information Engineering Systems, 1999. Third International Conference*. IEEE, 88–92.
- OpenFOAM Foundation. 2016. OpenFOAM Tutorials Lagrangian MPPICFoam cyclone. Official OpenFOAM Repository. <https://github.com/OpenFOAM/>. (November 2016).
- Thomas J Overcamp and Sridhar V Mantha. 1998. A simple method for estimating cyclone efficiency. *Environmental progress* 17, 2 (1998), 77–79.
- R Preen and L Bull. 2014. Towards the Coevolution of Novel Vertical-Axis Wind Turbines. *Evolutionary Computation, IEEE Transactions on PP*, 99 (2014), 284–294.
- Timothy Simpson, Vasilli Toropov, Vladimir Balabanov, and Felipe Viana. 2012. Design and Analysis of Computer Experiments in Multidisciplinary Design Optimization: A Review of How Far We Have Come - Or Not. In *12th AIAA/ISSMO Multidisciplinary Analysis and Optimization Conference*. American Institute of Aeronautics and Astronautics, Reston, Virginia, 1–22.
- Giulio Solero and Aldo Coghe. 2002. Experimental fluid dynamic characterization of a cyclone chamber. *Experimental thermal and fluid science* 27, 1 (Dec. 2002), 87–96.
- Matthew Staymates, Jerold Bottiger, Deborah Schepers, and Jessica Staymates. 2013. A Streamlined, High-Volume Particle Impactor for Trace Chemical Analysis. *Aerosol Science and ...* 47, 9 (Sept. 2013), 945–954.
- Prabhata K Swamee, Nitin Aggarwal, and Kuldeep Bhobhiya. 2009. Optimum design of cyclone separator. *AIChE journal* 55, 9 (Sept. 2009), 2279–2283.
- A J Turner, S Balestrini-Robinson, and D Mavris. 2013. Heuristics for the regression of stochastic simulations. *Journal of Simulation* 7, 4 (Feb. 2013), 229–239.
- Mark J. van der Laan and Sandrine Dudoit. 2003. *Unified cross-validation methodology for selection among estimators and a general cross-validated adaptive epsilon-net estimator: Finite sample oracle inequalities and examples*. Working paper 130. University of California, Berkeley, Division of Biostatistics, School of Public Health, University of California, Berkeley.
- David H Wolpert. 1992. Stacked generalization. *Neural Networks* 5, 2 (Jan. 1992), 241–259.
- Yuhong Yang. 2003. Regression with multiple candidate models: selecting or mixing? *Statistica Sinica* (2003), 783–809.
- Martin Zaefferer, Beate Breiderhoff, Boris Naujoks, Martina Friese, Jörg Stork, Andreas Fischbach, Oliver Flasch, and Thomas Bartz-Beielstein. 2014. Tuning Multi-Objective Optimization Algorithms for Cyclone Dust Separators. In *Genetic and Evolutionary Computation Conference (GECCO'14), Proceedings*. 1223–1230.
- Bernard P Zeigler and Tuncer I Oren. 1986. Multifaceted, Multiparadigm Modeling Perspectives: Tools for the 90's. In *Proceedings of the 18th Conference on Winter Simulation*. ACM, New York, NY, USA, 708–712.



---

## **Kontakt/Impressum**

Diese Veröffentlichungen erscheinen im Rahmen der Schriftenreihe "Ciplus". Alle Veröffentlichungen dieser Reihe können unter

<https://cos.bibl.th-koeln.de/home>  
abgerufen werden.

Köln, Januar 2012

Die Verantwortung für den Inhalt dieser Veröffentlichung liegt beim Autor.

Datum der Veröffentlichung: 12.12.2016

## **Herausgeber / Editorship**

Prof. Dr. Thomas Bartz-Beielstein,  
Prof. Dr. Wolfgang Konen,  
Prof. Dr. Boris Naujoks,  
Prof. Dr. Horst Stenzel  
Institute of Computer Science,  
Faculty of Computer Science and Engineering Science,  
TH Köln,  
Steinmüllerallee 1,  
51643 Gummersbach  
url: [www.ciplus-research.de](http://www.ciplus-research.de)

## **Schriftleitung und Ansprechpartner/ Contact editor's office**

Prof. Dr. Thomas Bartz-Beielstein,  
Institute of Computer Science,  
Faculty of Computer Science and Engineering Science,  
TH Köln,  
Steinmüllerallee 1, 51643 Gummersbach  
phone: +49 2261 8196 6391  
url: <http://www.spotseven.de>  
eMail: [thomas.bartz-beielstein@th-koeln.de](mailto:thomas.bartz-beielstein@th-koeln.de)

ISSN (online) 2194-2870

**Technology  
Arts Sciences  
TH Köln**

---

Supported by:



on the basis of a decision  
by the German Bundestag

Grant No. KF3145101WM3 and KF3145103WM4

---



This project has received funding from the European Union's Horizon 2020  
research and innovation programme under grant agreement No 692286.

---

**Technology  
Arts Sciences  
TH Köln**